Simulation of the Evolution of Pressure in a Lignite Particle during Pyrolysis

ARTICLE *in* ENERGY & FUELS · MAY 2014

Impact Factor: 2.79 · DOI: 10.1021/ef500584q

5 AUTHORS, INCLUDING:

He Yang
Dalian University of Technology
5 PUBLICATIONS **14** CITATIONS
SEE PROFILE

Sufen Li
Dalian University of Technology
18 PUBLICATIONS **52** CITATIONS
SEE PROFILE

Thomas H. Fletcher
Brigham Young University - Provo Main Campus
155 PUBLICATIONS **2,299** CITATIONS
SEE PROFILE

energy&fuels

Article

pubs.acs.org/EF

Simulation of the Evolution of Pressure in a Lignite Particle during Pyrolysis

He Yang,[†,‡] Sufen Li,*[,†] Thomas H. Fletcher,[‡] Ming Dong,[†] and Weishi Zhou[†]

[†]School of Energy and Power Engineering, Dalian University of Technology, Dalian, Liaoning 116024, People's Republic of China

[‡]Chemical Engineering Department, Brigham Young University, Provo, Utah 84602, United States

ABSTRACT: The evolution of pressure in a lignite particle during pyrolysis was simulated on the basis of the gas motion equation in porous media and considering the Klinkenberg effect. The chemical percolation devolatilization (CPD) model was used to describe pyrolysis. The pore diameter in the particle is close to the average free path of volatile gas molecules; therefore, the solid phase restrains the movement of gas. Because flow out of the particle is restricted, the internal pressure rises. The internal pressure first increases and then decreases during pyrolysis, and the evolution is influenced by heating conditions. The pressure rise is larger at a higher heating rate, but the duration of the pressure peak is shorter. The total pressure in the particle is larger at a higher ambient pressure, but the pressure difference between the inside and the surroundings decreases with the increasing ambient pressure. A growing internal pressure can restrain tar gasification, which can lead to the increase of the Metaplast content and the decline of the tar yield.

1. INTRODUCTION

In commercial entrained-flow boilers and gasifiers, lignite particles are heated at 10^6 K/s with pressures of 3.0−6.0 MPa in gasifiers.[1] Large amounts of gases are generated from pyrolysis within a short time. Because the pore diameter in the particle is close to the average free path of volatile gas molecules, the solid phase restrains the movement of gases. Flow out of the particle is therefore restricted, and some gases are amassed in the pores,[2,3] making the pressure in the particle rise higher than the surroundings. The internal pressure is not only controlled by the heating rate and surrounding pressure but may also influence the pyrolysis reactions directly. Therefore, a description of the evolution of internal pressure is important to analyze the influence of experimental conditions on pyrolysis.

In most studies on pyrolysis, pressure inside the particle is regarded as equal to the surrounding pressure. However, at rapid heating rates and elevated pressure, ignoring internal pressure will reduce the accuracy of the model and make it hard to analyze the volatile transport.[4] Recent studies on pyrolysis at a high temperature and an elevated pressure have focused on the influence of experimental conditions on the final yield and particle size[5] but have not treated the evolution of internal pressure and its influence on chemical reaction.

In this paper, the evolution of pressure in a North Dakota Beulah Zap lignite particle during pyrolysis is simulated according to the gas motion equation in porous media to analyze the formation of internal pressure and its influence on reaction. A lignite was selected because the observed changes in particle size during pyrolysis are small for this type of coal. Modeling pressures in swelling coal particles is more complicated and a subject of ongoing research.

2. MODELING

In lignite pyrolysis, the light gas and tar are generated following the breakup of the macromolecular network.[6,7] Because the pore diameter in the particle is close to the average free path of volatile gas molecules, the flow out of the particle is restricted. During rapid pyrolysis, a large amount of gas is accumulated in the particle, which, in turn, increases gas density and internal pressure. Meanwhile, the pressure gradient in the particle also increases, and gases flow out of the particle faster. Unsteady distributions of pressure, density, and velocity occur in the particle during pyrolysis. To obtain the evolution of internal pressure during pyrolysis, the coupling of velocity and pressure in the particle must be solved.

2.1. Assumptions. (1) The coal particle is spherical and isotropic; therefore, pressure and velocity of gas only change in the radial direction, and there is no pressure or velocity gradient in the circumferential direction. (2) The coal particle is a porous media with continuous cylindrical pores with no fragmentation or thermoplastic deformation during pyrolysis. This assumption is better for a lignite than for a swelling coal.

2.2. Control Equation. *2.2.1. Pyrolysis Reaction Model.* The pyrolysis reaction is mainly described by the chemical percolation devolatilization (CPD) model.[7] The CPD model includes (a) a description of the chemical structure of the parent coal, (b) a kinetic scheme for breaking labile bonds and side chains, (c) percolation statistics based on a Bethe lattice for freeing molecules from the coal particle, (d) a vapor−liquid equilibrium treatment of Metaplast versus tar, and (e) a cross-linking mechanism for reattaching Metaplast to the solid char. The average internal pressure in the particle obtained by the computational fluid dynamics (CFD) method is used as the reaction pressure in the CPD model instead of the external pressure. The distribution of tar and most light gases is calculated by the CPD model.[8] The paraffin/olefin ratio for noncondensable gases during coal pyrolysis was measured by Serio et al.[9] This ratio was used to split the "other gases" category from the CPD model into the yield of noncondensable paraffins and olefins.

2.2.2. Gas Differential Continuity Equation in Porous Media. In spherical coordinates, the gas continuity equation in porous media is described as

Received: March 18, 2014
Revised: April 18, 2014
Published: April 21, 2014

   dx.doi.org/10.1021/ef500584q | *Energy Fuels* 2014, 28, 3511−3518

$$\theta\frac{\partial\rho}{\partial t} + \frac{1}{r^2}\frac{\partial(\rho r^2 U)}{\partial r} - \frac{dm}{dt} = 0 \quad (1)$$

where U is the average velocity through the sphere of radius r, m is the yield of volatiles at time t, and the porosity is estimated by $\theta = \theta_0 + (1 - \theta_0)m$ based on the assumption that porosity has a linear relationship with weight loss.

2.2.3. Gas Differential Equations of Motion in Porous Media. In spherical coordinates, the differential equation of gas motion in porous media is shown in eq 2

$$\theta^{-1}\frac{\partial\rho U}{\partial t} + \theta^{-2}U\frac{\partial\rho U}{\partial r} = -\frac{\mu}{K}U - \frac{1}{r^2}\frac{\partial(pr^2)}{\partial r} \quad (2)$$

where p is the pressure, μ is the viscosity of volatile gas, and K is the permeability.

When the average free path of the volatile gas molecules is close to the pore diameter, the gas molecular slippage on the surface of pore walls caused by the collision between gas molecules and pore walls becomes an important part of gas movement, which is called the Klinkenberg effect.[10] To consider this effect, K is expressed as shown in eq 3

$$K = K_0(1 + 29/3e^{-2r_k/\bar{\lambda}}) \quad (3)$$

where the absolute permeability $K_0 = \theta/8r_k^2$, the pore radius $r_k = 2r_f\theta/S$, where r_f is the roughness factor,[11] and the average free path of molecule $\bar{\lambda}$ is described as

$$\bar{\lambda} = \frac{kT}{\sqrt{2}\,\pi d_{mol}^2 p} \quad (4)$$

where k is the Boltzmann constant and d_{mol} is average molecular diameter of gases.

A sample calculation was performed to illustrate the importance of the Klinkenberg effect. During the lignite particle pyrolysis described in this paper at an ambient pressure of 0.1 MPa and a heating rate of 10^4K/s, the permeability K doubles after 60 ms compared to K_0 because of the Klinkenberg effect, as shown in Figure 1.

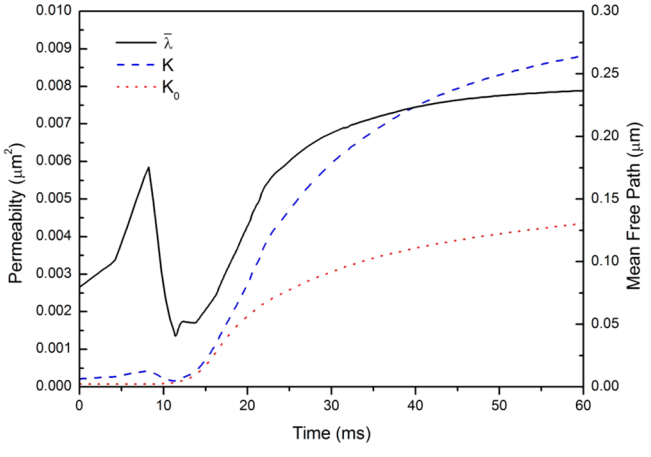

Figure 1. Evolution of K_0, K, and $\bar{\lambda}$ during pyrolysis.

2.3. Average Gas Molecular Diameter and Molecular Weight. The average molecular diameter of gases is estimated as

$$\bar{d}_{mol}(t) = \frac{\sum(dn_i(t) + n_i^a(t))d_{mol}^i}{\sum[dn_i(t) + n_i^a(t)]} \quad (5)$$

where d_{mol}^i is the molecular diameter of species i, $dn_i(t)$ is the amount of species i generated at time t, and $n_i^a(t)$ is the amount of species i accumulated in the particle at time t

$$n_i^a = \int_0^t \left(\frac{dn_i}{dt} - \frac{dn_i^e}{dt}\right)dt \quad (6)$$

where n_i^e is the amount of species i flowing out of the particle and $dn_i^e/dt = Q_e/\bar{M}_v$. Q_e is the mass flow rate out of the particle boundary. The average molecular weight of gases is expressed as shown in eq 7

$$\bar{M}_v(t) = \sum\left(\frac{dn_i(t) + n_i^a(t)}{\sum[dn_i(t) + n_i^a(t)]}\right)M_v^i \quad (7)$$

2.4. Initial and Boundary Conditions. The initial conditions are at $t = 0$, $p = p_\infty$, and $U = 0$, where p_∞ is the ambient pressure. The boundary conditions become

$$\begin{cases} t > 0:\ r = 0,\ U = 0,\ \dfrac{\partial p}{\partial r} = 0 \\ t > 0:\ r = r_p,\ p = p_\infty \end{cases} \quad (8)$$

2.5. Calculation Conditions. Pyrolysis of a 60 μm North Dakota Beulah Zap lignite particle is simulated. The heating conditions are the same as the coal pyrolysis experiment by Serio et al.[9] The results of simulation are compared to the results of the experiment to verify the accuracy of the model.

In addition, the pyrolysis of the lignite particle at various heating rates and ambient pressures are simulated. To simplify, it is assumed the particles are heated at a constant heating rate to 1050 K to analyze the effects of gas accumulation on various conditions.

Coal parameters for the CPD model calculations are shown in Table 1.

Table 1. Coal Parameters[a]

C_{daf} (%)	A_{ad} (%)	θ_0	p_0	c_0	M_{clust}	M_δ	$\sigma + 1$
66.5	6.2	0.13	0.59	0.10	410	51	5.2

[a] $\sigma + 1$ represents the coordination number. M_{clust} and M_δ represent the molecular weights of the cluster and side chain, respectively. C_{daf} represents the carbon content on a dry and ash-free basis. A_{ad} represents the ash content on an analysis basis. θ_0 represents the initial porosity. p_0, c_0, and δ_0 represent the initial population of intact bridges, population of char bridges, and population of side chains on a per bridge basis, respectively. $\sigma + 1$, p_0, δ_0, M_{clust}, and M_δ are obtained from the related experiment data, and c_0 is calculated from the correlation developed for use with the CPD model.[12]

3. GRIDS AND DISCRETE SCHEME

3.1. Grids. To solve the coupling problem of velocity and pressure in the particle, the staggered grids are adopted, as shown Figure 2. The particle is divided into 301 pressure grids

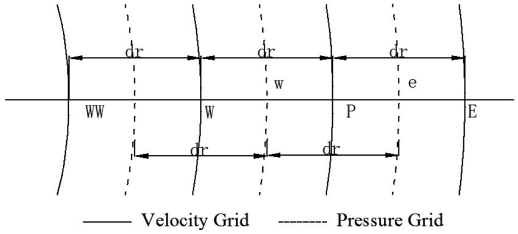

Figure 2. Schematic of staggered grids.

and 300 velocity grids in the radial direction. Pressure and velocity grids are staggered; the grid spacing is 0.1 μm, and the first point of pressure grids is the center of the sphere.

3.2. Discretization Scheme. A second-order upwind discrete differencing scheme was adopted. Equation 2 can be expressed as eq 9

dx.doi.org/10.1021/ef500584q | Energy Fuels 2014, 28, 3511−3518

$$\left[\frac{3}{2}F_e + a_p^0 + \frac{\mu}{K}\Delta V\right]U_p = \left[\frac{3}{2}F_w + \frac{1}{2}F_e\right]U_w - \frac{1}{2}F_wU_{ww} + a_p^0U_p^0 + A_p(p_w - p_e) \quad (9)$$

where $F = \rho UA\theta^{-2}$ and $a_p^0 = \theta^{-1}(\rho\Delta V/\Delta t)$.

To solve the coupling problem of velocity and pressure in the particle, the SIMPLE algorithm was adopted, letting p^* represent the hypothetical pressure, U^* represent the hypothetical velocity, ρ_p^* represent the hypothetical density, p' represent the correction value of pressure, U' represent the correction value of velocity, and ρ_p' represent the correction value of density in one loop step ($p = p^* + p'$, and $U = U^* + U'$). Equation 1 can be expressed as eq 10

$$\left[(\rho UA)_w + (\rho UA)_e + \frac{\theta\Delta V}{R_gT\Delta t}\right]p_p' = (\rho UA)_wp_w' + (\rho UA)_ep_e' + (\rho U^*A)_w - (\rho U^*A)_e - \frac{\theta(\rho_p^* - \rho_p^0)\Delta V}{\Delta t} + dm \quad (10)$$

where $\rho_p' = p_p'/R_gT$.

3.3. Average Internal Pressure. According to the pressure distribution in the particle and the size of each control unit, the average internal pressure can be obtained by the volume mean, as shown in eq 11

$$\bar{p}(t) = \frac{\sum p_n(t)V_{k,n}(t)}{\sum V_{k,n}(t)} \quad (11)$$

where $p_n(t)$ and $V_{k,n}(t)$ represent the pressure in control unit n and the corresponding volume, respectively.

3.4. Independence of the Grid Size. Results obtained from grid spacings of 0.1 μm (301 grids in the radial direction), 0.01 μm (3001 grids in the radial direction), and 0.5 μm (61 grids in the radial direction) are compared, as shown in Figure 3. The maximum relative deviation of the average internal pressure between the 0.1 and 0.01 μm grid spacing cases was 0.22%, and that between the 0.1 and 0.5 μm grid spacing cases was 2.4%. The grid spacings of 0.1 and 0.5 μm were both small enough to obtain an accurate internal pressure. However, to obtain a more accurate result of gas accumulation and analyze the influence of the internal pressure on the yield of volatiles, the grid spacing of 0.1 μm was adopted in this paper.

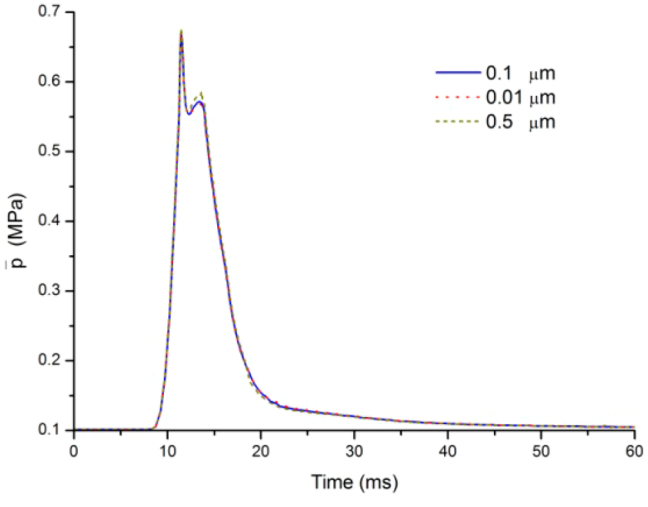

Figure 3. Test of grid independence.

3.5. Convergence Condition. The convergence condition is $p'/p < 10^{-12}$ at all grid points in one time step.

4. RESULTS AND DISCUSSION

4.1. Model Validation. The yields of volatiles in the simulation are compared to the experiment by Serio et al.[9] to verify the accuracy of the model. The simulation results agree well with the experimental results, as shown in Figure 4.

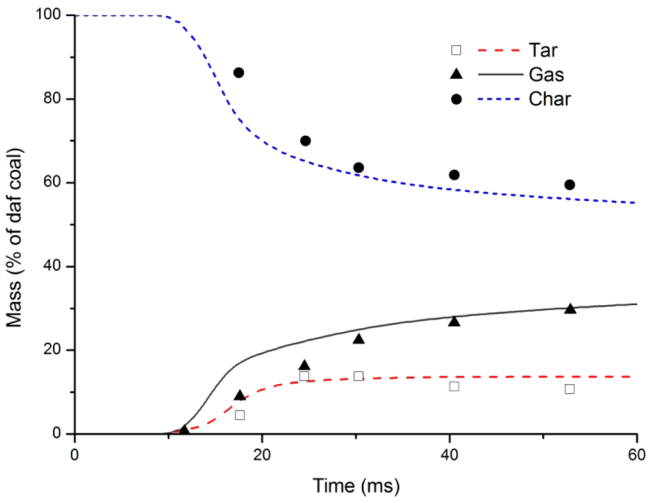

Figure 4. Comparison of the predicted yields to data from the experiment by Serio et al.

4.2. Formation Mechanism of Internal Pressure. The pore radius (r_{pore}) in the particle is close to the average free path of volatile gas molecules, as shown in Figure 5. Collisions between molecules and pore walls restrain gas movement. The volatile gas cannot flow out of the particle as soon as the gas is generated and, therefore, accumulates in the particle.

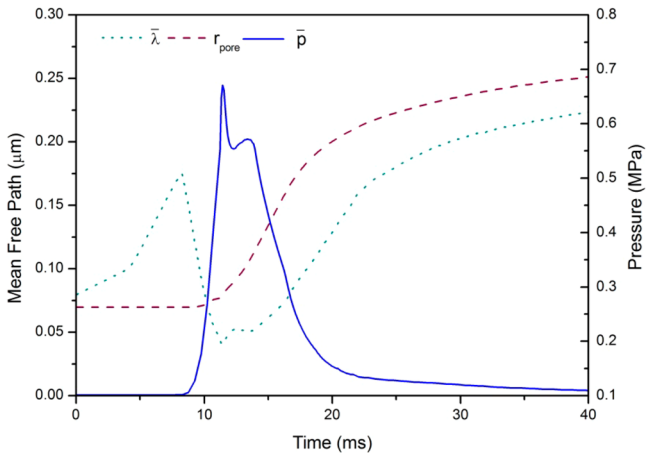

Figure 5. Evolution of $\bar{p}$, r_{pore}, and $\bar{\lambda}$ for the experiment by Serio et al.

The free path of gas molecules can indicate the concentration of gas molecules. A small free path means that the concentration is large. At the beginning of heating, before pyrolysis, with the increase of the temperature, the density of

dx.doi.org/10.1021/ef500584q | Energy Fuels 2014, 28, 3511−3518

gas declines and free path is increased. However, as soon as the pyrolysis starts, some part of the new generated gases is accumulated in the particle and the collision frequency of gas molecules increases; therefore, the free path declines rapidly. After the peak in pressure, with the decrease of gas accumulation, the free path is increased and fluctuates with fluctuations of pressure.

The evolution of the moles of light gas and tars of different mer sizes accumulated in the coal particle is shown in Figures 6 and 7. Note that the tar consists mainly of monomers, with some dimers and trimers and relatively few higher molecular weight clusters.

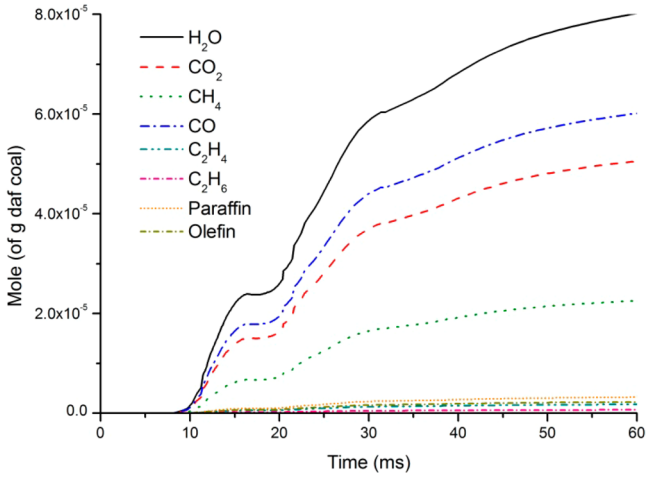

Figure 6. Evolution of moles of various light gases accumulated in the coal particle during pyrolysis for the experiment by Serio et al.

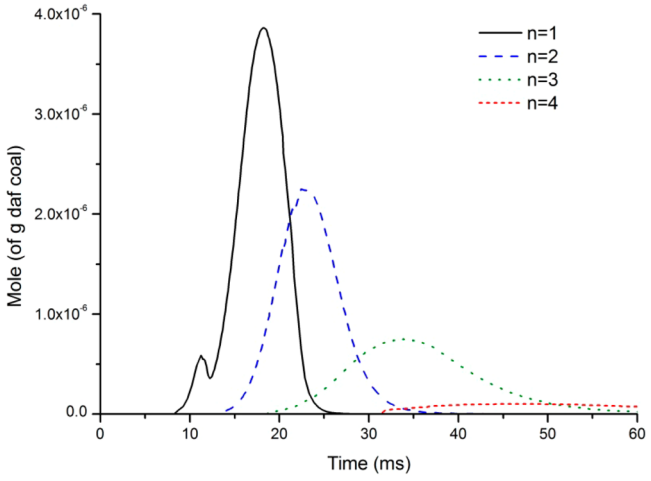

Figure 7. Evolution of moles of various tars accumulated in the coal particle during pyrolysis for the experiment by Serio et al. (*n* represents the number of aromatic clusters per finite molecular fragment in CPD mode).

The moles of light gases accumulated in the particle are much larger than that of tar because the total moles of light gases generated is much larger than that of tar for this coal. The large number of moles of light gas helps push the tar out of the particle and eventually totally occupy the pore spaces. However, the tar molecular weight is much larger than the light gases; therefore, tar accumulation influences the average gas molecular weight in the particle and makes the average gas molecular weight fluctuate, as shown in Figure 8.

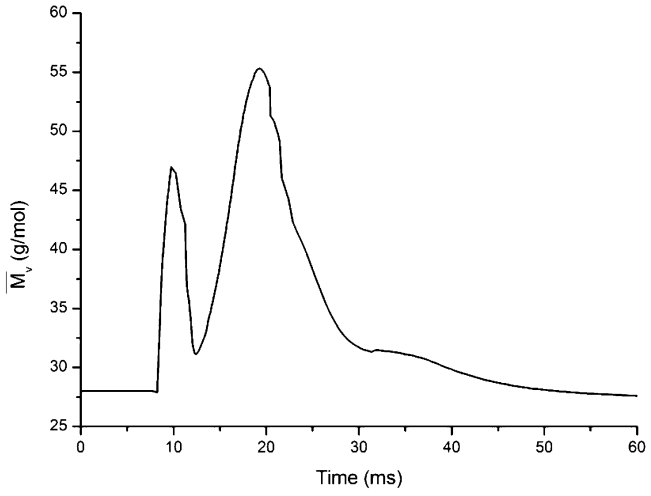

Figure 8. Evolution of the average gas molecular weight during pyrolysis in the particle for the experiment by Serio et al.

At the beginning of pyrolysis, some aromatic clusters not initially connected with the coal matrix evaporate at early residence times to form the tar. At this stage, the tar accumulation is increased rapidly. During this region of rapid tar release, the molecular weight of gases increases rapidly. As the generation rate of tar declines, the tar accumulation decreases (see Figure 7). Meanwhile, as light gases are generated, the number of gas molecules increases; therefore, the molecular weight decreases. However, at higher temperatures, the aliphatic bridges between the aromatic clusters thermally decompose and the generation rate of tar is increased. Because tar is generated in this stage with multiple clusters, the molecular weight is increased again. Finally, after the generation of tar is completed, the molecular weight decreases.

4.3. Changes in Internal Pressure in Coal. Restrained by solid structure, molecules cannot pass through pores freely. The gas concentration inside the particle is much larger than outside the particle, and hence, the pressure increases from the boundary to the core of the particle, as shown in Figure 9. The

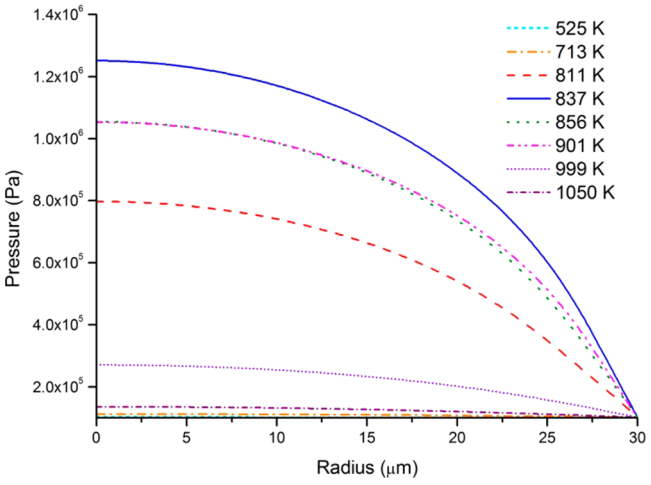

Figure 9. Pressure distribution in the radial direction for the conditions of the experiment by Serio et al.

dx.doi.org/10.1021/ef500584q | *Energy Fuels* 2014, 28, 3511−3518

internal pressure first increases and then decreases during the heating process. When the particle temperature reaches 837 K, the internal pressure is at a maximum and the pressure at the core of the particle is 1.25×10^6 Pa.

The change in the internal pressure is mainly controlled by the increase and decrease of the gas generation rate. At a higher generation rate, more volatile gases are accumulated in the particle and the internal pressure is larger. The evolution of the average internal pressure $\bar{p}$ and generation rate of volatiles dm/dt for the experiment by Serio et al. is shown in Figure 10.

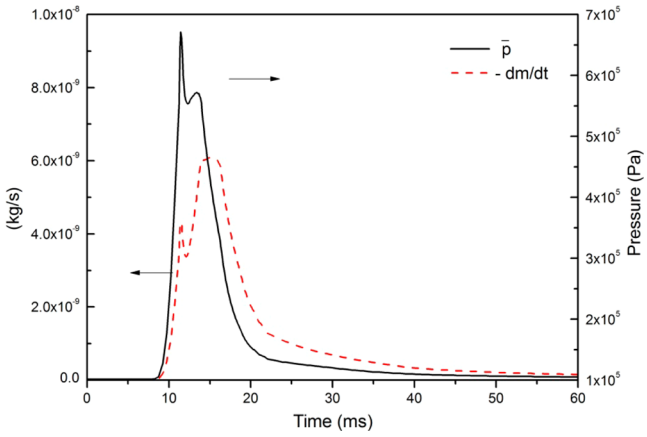

Figure 10. Changes in $\bar{p}$, dm/dt, and Q_e during pyrolysis for the experiment by Serio et al.

The evolution of the internal pressure is also influenced by the change of the pore size and pressure–velocity coupling during pyrolysis. Changes in the pore size make the changes in the internal pressure not completely synchronized with the changes in the gas generation rate. During pyrolysis, with the expansion of pores, the permeability increases, which enhances the ability for more gases to flow out of the particle. Therefore, the increase in the internal pressure is smaller in the later stages of the reaction, even if the generation rate is larger, and the internal pressure decreases before the decline of the generation rate. Meanwhile, because various components are generated at different times, the fluctuating average gas molecular weight causes time-dependent fluctuations in the internal pressure. At the first peak of internal pressure, the average gas molecular weight is decreasing; therefore, the internal pressure increases rapidly, and the peak is sharp. However, at the second peak, the average gas molecular weight is rising; therefore, the internal pressure increases more slowly, and the peak is more rounded with a more gradual decay.

4.4. Influence of the Heating Rate on Internal Pressure. The internal pressure is larger at a higher heating rate, but the duration of the pressure peak is shorter. Transient internal pressure profiles at an ambient pressure of 0.1 MPa and various heating rates are shown in Figure 11. At a heating rate of 5×10^3 K/s, the maximum average internal pressure is only 0.2 MPa and the duration of pressure larger than 0.11 MPa is 81 ms. However, at a heating rate of 5×10^5 K/s, the maximum average internal pressure increases by 2.54 MPa, which is 25.4 times larger than the ambient pressure, but the duration of the pressure larger than 0.11 MPa is only 16.6 ms.

The relationship between the mass release, temperature, and time varies with the heating rate during pyrolysis.[13,14] With an increasing heating rate, mass release occurs at higher temperatures, which makes the peaks of the reaction and internal pressure move to a higher temperature region. The reaction at higher temperatures causes the following effects: (1) Reaction is concentrated into a shorter time; therefore, more gas is produced in a shorter time. Gases are generated faster than they can flow out of the particle. The accumulation of gas is therefore increased, and the local pressure is elevated. (2) At a higher temperature, the free path of the volatile gas molecules is larger; therefore, the frequency of gas molecule collisions is larger at a certain volume. The pressure is therefore further increased (i.e., by a temperature rise in a gas with a constrained volume). (3) The increased pressure rise in the particle increases the driving force for gases to flow out of the particle and reduces the residence time of gases inside the particle.

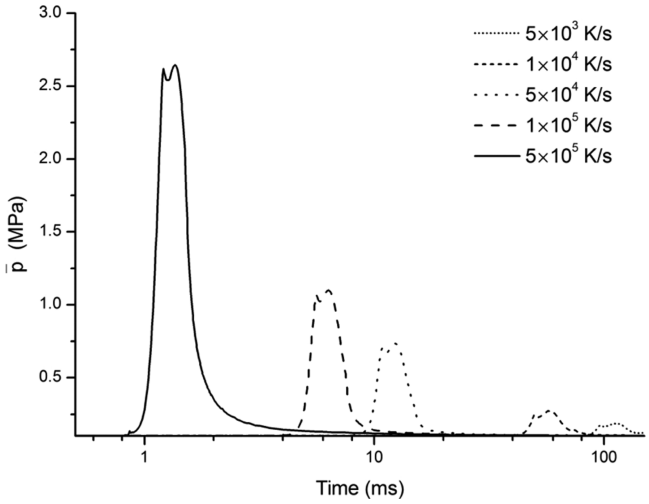

Figure 11. Transient internal pressure profiles at various heating rates and an ambient pressure of 0.1 MPa (where $\bar{p}$ is the difference between the internal pressure and the ambient pressure).

Faster gas accumulation makes internal pressure increase, but the duration of the accumulation affect decreases with increases in the heating rate.

4.5. Influence of External Pressure. The total pressure in the particle is larger at a higher ambient pressure, but the pressure difference between the inside and the surrounding decreases slightly with the increasing ambient pressure. For example, transient profiles of the difference between the internal pressure and the ambient pressure at a heating rate of 10^4 K/s and various ambient pressures are shown in Figure 12. At 0.1 MPa, the peak pressure difference was 0.17 MPa but was 0.15 MPa at 0.3 MPa.

The increase in pressure can restrain the vaporization of Metaplast and cause a decrease in the tar yield. This causes a smaller amount of tar to change phase, which, in turn, decreases the pressure difference between the inside and outside of the particle.

The influence of ambient pressure on internal pressure is mainly caused by its effect on the amount of gases in the particle and the free path of molecules. Elevating ambient pressure can increase the total pressure in the particle. The amount of gas molecules increases, and the free path of the volatile gas molecules decreases, as shown in Figure 13. The collision frequency between the molecule and the pore wall is reduced relative to that between molecules. The restraint on freedom of molecular motion by the solid is reduced relatively;

dx.doi.org/10.1021/ef500584q | Energy Fuels 2014, 28, 3511–3518

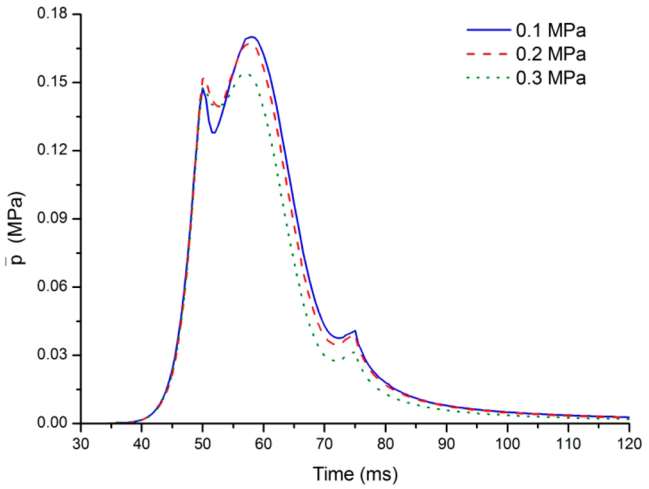

Figure 12. Time-dependent difference between internal and ambient pressure at 10^4 K/s and various ambient pressures.

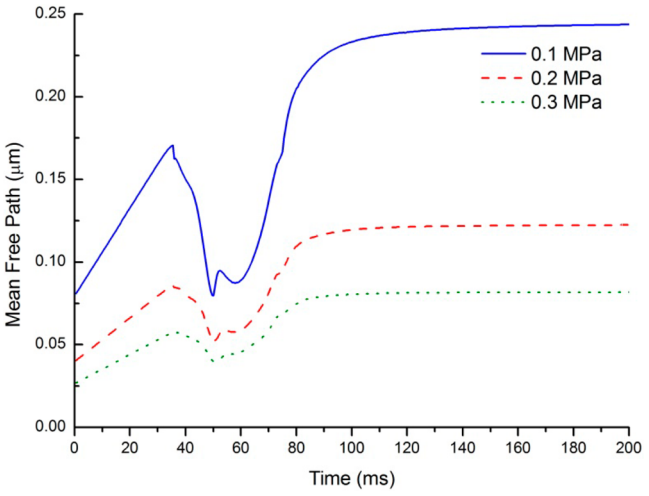

Figure 13. Free path of gas molecules at various pressures for a heating rate of 10^4 K/s.

therefore, the pressure differences between inside and outside of the particle decline.

4.6. Rationale for the Assumption of No Fragmentation or Thermoplastic Deformation. The diameter of North Dakota Beulah Zap lignite changes little during pyrolysis.[1,15] Plastic deformation only happens when the viscosity of the particle is smaller than the critical viscosity. A correlation to calculate the viscosity is as shown in eq 12, and the critical viscosity is 1×10^4 Pa s[13]

$$\mu = \frac{1 \times 10^{-11} \exp(45000/RT)}{((1 - \phi_m)^{-1/3} - 1.0)} \quad (12)$$

where ϕ_m is the Metaplast content in the coal melt, where T is set to 723 K when $T > 723$ K. On the basis of eq 12, the minimum viscosity of the particle during pyrolysis is 1.005×10^4 Pa s at a heating rate of 10^4 K/s and an ambient pressure of 0.3 MPa, which is still slightly larger than the critical viscosity. This value of 1.005×10^4 Pa s is the smallest viscosity for all of the calculations presented in this paper.

In addition, the maximum average pressure difference between the inside and outside of the particle during pyrolysis at various heating conditions in the paper is 2.54 MPa, which is much smaller than the coal tensile stress strength (4.4 MPa) reported by Chirone and Massimilla.[16]

4.7. Influence of the Internal Pressure on Pyrolysis. Internal pressure influences the phase equilibrium in the particle. The increase of pressure can restrain the vaporization of Metaplast, which can increase the amount of Metaplast and, therefore, increase cross-linking reactions, which will decrease the yield of tar. A set of computations was performed that used the ambient pressure for the devolatilization model instead of the local instantaneous internal pressure (see Figure 14).

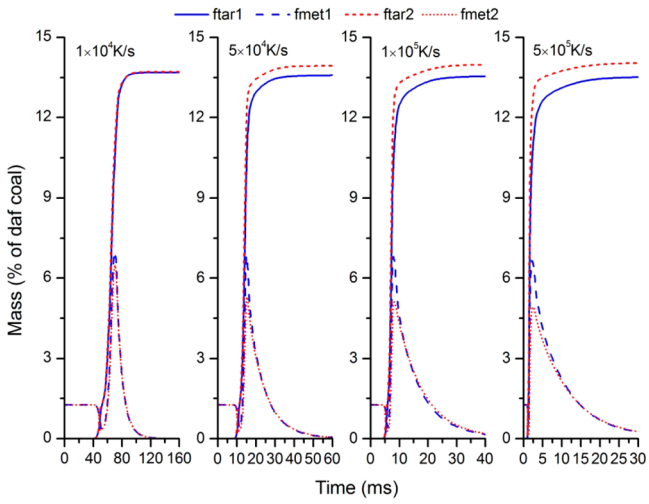

Figure 14. Evolution of tar (ftar) and Metaplast (fmet) during pyrolysis at various heating rates. (ftar1 and fmet1 are from using the local instantaneous internal pressure for the devolatilization model, and ftar2 and fmet2 are from using the ambient pressure).

Computations were performed at four different heating rates. Solid curves with labels ending in "1" were for the computations considering the local instantaneous internal pressure for the devolatilization model, while dashed curves with labels ending in "2" were for the cases where the ambient pressure was used for the devolatilization model. As seen in Figure 14, the yield of tar calculated by the model considering the effects of the internal pressure is slightly smaller and the content of Metaplast is larger but the effect is negligible at the lower heating rate (10^4 K/s). However, with the increasing heating rate, a larger internal pressure occurs and the effect of the internal pressure becomes more obvious. For example, at a heating rate of 5×10^5 K/s, the maximum value of Metaplast changed from 4.9 to 6.7%, which is a relative difference of 36%. Small changes in tar yield are also seen at the higher heating rates in Figure 14.

4.8. Internal Surface Area. The internal surface area of a lignite particle usually remains constant at the beginning of pyrolysis but then increases significantly during later stages of pyrolysis. This increase in internal surface area can be explained by the evolution of the number of micropores in the particle during pyrolysis. Along with breakup of the macromolecular network, the spaces left by the light gas molecules between aromatic clusters form micropores. However, along with the generation of tar, some micropores attached to the aromatic clusters will be removed from the particle. Therefore, during tar release, the amount of micropores in the particle does not increase significantly and only slight changes occur in the internal surface area. After the tar generation stops, a large

dx.doi.org/10.1021/ef500584q | Energy Fuels 2014, 28, 3511−3518

number of micropores are formed because of light gas release and the internal surface area increases significantly.

A correlation was established to predict the evolution of N_2 Brunauer–Emmett–Teller (BET) surface area of a lignite particle during pyrolysis as shown in eq 13

$$S_{bet} = a_m N_A \left[\frac{g_1}{2} \left(\frac{g_1}{\delta + g_1} \right) \left(\frac{1}{M_{clust}} - N_{clust-tar} \right) \left(\frac{\sigma + 1}{2} \right) + S^0_{bet} \left(1 - \frac{N_{clust-tar}}{1/M_{clust}} \right) \right] \quad (13)$$

where a_m is the cross-sectional area of a N_2 molecule, N_A is the Avogadro constant, S^0_{bet} is the initial BET surface area of the coal particle, g_1, δ, and M_{clust} are the parameters from the CPD model and represent the population of gases formed from side chains, the population of side chains, and the molecular weight per aromatic cluster, respectively, and $N_{clust-tar}$ is the population of clusters taken out of the particle by evaporation of tar.

A comparison of the correlation with experimental data for Beulah Zap lignite[15,17] and Glen Harold Mine lignite[18] is shown in Figure 15.

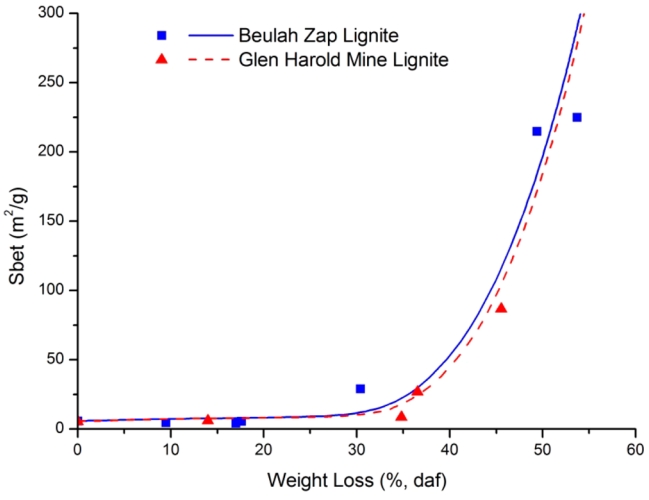

Figure 15. Comparison of N_2 BET surface area correlation with experiment data from Fletcher and Hardesty[15] and Nsakala et al.[18] The curve is the prediction, and the data points are the data.

Although the internal surface area increased significantly during the later stages of pyrolysis [greater than 30% dry and ash-free (daf) weight loss], most of the change in internal surface occurred because of increases in the number of micropores. However, most of the flow does not occur in the micropores, so that the effects on the permeability are small. In the simulation in this paper, the internal surface area was set at a constant 5 m^2/g.

4.9. Influence of Coal Parameters on Internal Pressure. The evolution of pressure in the Beulah Zap lignite and Glen Harold Mine lignite particles during pyrolysis at a heating rate of 5×10^5 K/s is compared in Figure 16. The volatile yields for these two lignites are shown in Figure 17. Table 2 is a comparison of the parameters for the two coals, where the parameters of Glen Harold Mine lignite were calculated from the correlation developed for use with the CPD model.[12] The main difference between the parameters for the two coals is that the Glen Harold Mine lignite has smaller

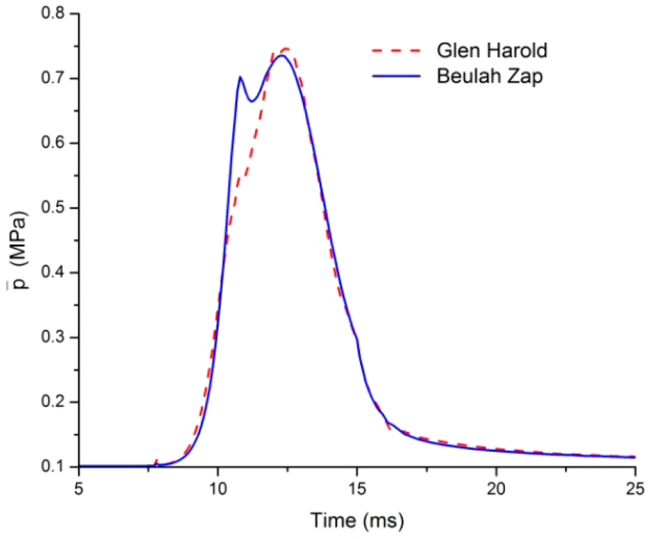

Figure 16. Comparison of evolution of pressure in the particles of Beulah Zap lignite and Glen Harold Mine lignite during pyrolysis at a heating rate of 5×10^5 K/s.

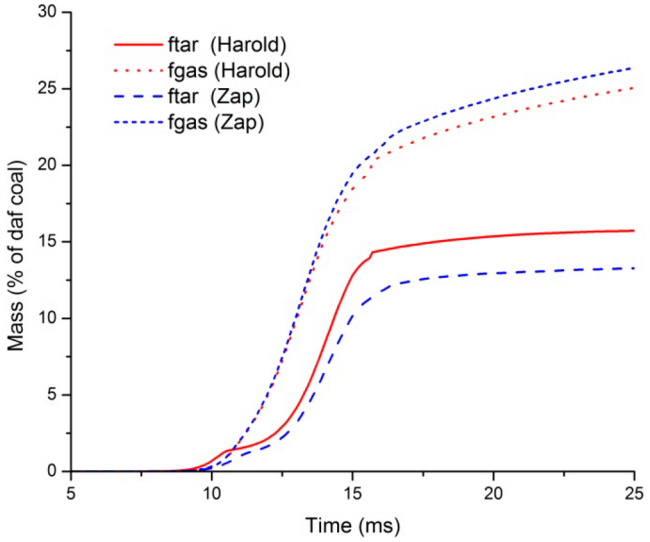

Figure 17. Comparison of volatile yields for Beulah Zap lignite and Glen Harold Mine lignite during pyrolysis at a heating rate of 5×10^5 K/s.

Table 2. Coal Parameters

	p_0	c_0	M_{clust}	M_δ	$\sigma + 1$
Beulah Zap	0.59	0.1	410	51	5.2
Glen Harold Mine	0.60	0.13	342	45	4.8

values for the coordination number and the molecular weights of clusters and side chains.

The smaller coordination number means tar can be produced with fewer broken bridges; therefore, the generation of tar for the Glen Harold Mine lignite started slightly earlier than that for the Beulah Zap lignite, as shown in Figure 17. The earlier release of tar and light gases for the Glen Harold Mine lignite spreads the accumulation over more time, decreasing the concentration at the beginning of pyrolysis; therefore, the first peak of internal pressure for this lignite is barely observable, as shown in Figure 16. Note that the first pressure peak (or the shoulder for the Glen Harold Mine lignite) occurred at about

dx.doi.org/10.1021/ef500584q | Energy Fuels 2014, 28, 3511–3518

10.5 ms, which corresponds to a total volatile yield of about 2% of the daf coal. The second pressure peak was slightly higher for the Glen Harold Mine lignite, which is caused by the smaller molecular weight of clusters and side chains. Smaller molecular weights for similar amounts of mass mean a larger number of molecules, which raises the internal pressure.

5. CONCLUSION

During lignite pyrolysis, the pore diameter in the particle is close to the average free path of volatile gas molecules. Because of diffusion resistance through the pores in the solid, some of the gases accumulate in the particle, elevating the internal pressure. The internal pressure increases first and then decreases during pyrolysis. The change in internal pressure is mainly controlled by the gas generation rate and is also influenced by the change of the pore size and pressure−velocity coupling during pyrolysis.

The pressure rise is larger at a higher heating rate, but the duration of the pressure peak is shorter. At a heating rate of 5×10^3 K/s and an ambient pressure of 0.1 MPa, the maximum calculated average internal pressure is only 0.2 MPa and the duration of the pressure larger than 0.11 MPa is 81 ms. However, at a heating rate of 5×10^5 K/s and 0.1 MPa ambient pressure, the maximum calculated pressure difference reached 2.54 MPa but the duration of pressure larger than 0.11 MPa is only 16.6 ms.

The total pressure in the particle is larger at a higher ambient pressure, but the pressure difference between the inside and the surroundings decreases slightly with the increasing ambient pressure. At a heating rate of 10^4 K/s and 0.1 MPa, the peak pressure difference was 0.17 MPa but was 0.15 MPa at 0.3 MPa.

Increasing internal pressure can restrain tar release because of vapor pressure considerations, which can lead to the increase in the mass of Metaplast and the decline of the tar yield. At a heating rate of 5×10^5 K/s, the maximum amount of Metaplast increased from 4.9 to 6.7% (36% on a relative basis) when the internal pressure was used for the devolatilization model instead of the ambient pressure. Slight decreases in the tar yield were also predicted when the internal pressure was used in the devolatilization calculations instead of the ambient pressure.

AUTHOR INFORMATION

Corresponding Author

*E-mail: lisuf@dlut.edu.cn.

Notes

The authors declare no competing financial interest.

ACKNOWLEDGMENTS

This work is supported in part by a scholarship from the China Scholarship Council (CSC) under Grant CSC 201306060059 and partially performed at Brigham Young University when He Yang was a visiting graduate student.

REFERENCES

(1) Shurtz, R. C.; Kolste, K. K.; Fletcher, T. H. Coal swelling model for high heating rate pyrolysis applications. *Energy Fuels* **2011**, *25*, 2163−2173.

(2) Yu, Y.; Xu, M.; Yu, D.; Huang, J. Fragmentation of coal particles by devolatilization during combustion. *J. Huazhong Univ. Sci. Technol.* **2005**, *3*, 78−80.

(3) Wu, Z.; Zhang, C. l.; Chen, H. Establishment of fragment model of coal during combustion. *J. Fuel Chem. Technol.* **2003**, *31* (1), 17−21.

(4) Fu, W.; Yu, W. Application of general devolatilization model of pulverized coal under changeable surrounding temperature. *J. Eng. Thermophys.* **1991**, *1*, 91−95.

(5) Shurtz, R. C. Effects of pressure on the properties of coal char under gasification conditions at high initial heating rates. Ph.D. Dissertation, Chemical Engineering, Brigham Young University, Provo, UT, 2011.

(6) Solomon, P. R.; Hamblen, D. G.; Yu, Z. Z.; Serio, M. A. Network models of coal thermal-decomposition. *Fuel* **1990**, *69* (6), 754−763.

(7) Fletcher, T. H.; Kerstein, A. R.; Pugmire, R. J.; Solum, M. S.; Grant, D. M. Chemical percolation model for devolatilization. 3. Direct use of ^{13}C NMR data to predict effects of coal type. *Energy Fuels* **1992**, *6* (4), 414−431.

(8) Genetti, D. B. An advanced model of coal devolatilization based on chemical structure. M.S. Thesis, Chemical Engineering Department, Brigham Young University, Provo, UT, 1999.

(9) Serio, M. A.; Hamblen, D. G.; Markham, J. R.; Solomon, P. R. Kinetics of volatile product evolution in coal pyrolysis: Experiment and theory. *Energy Fuels* **1987**, *1* (2), 138−152.

(10) Chen, D. Gas slippage phenomenon and change of permeability when gas flowes in tight porous media. *Acta Mech. Sin.* **2002**, *1*, 96−100.

(11) Ma, L. Combustion and gasification of chars in oxygen and carbon dioxide at elevated pressure. Ph.D. Thesis, Mechanical Engineering, Stanford University, Stanford, CA, 2006.

(12) Genetti, D.; Fletcher, T. H.; Pugmire, R. J. Development and application of a correlation of ^{13}C NMR chemical structural analyses of coal based on elemental composition and volatile matter content. *Energy Fuels* **1999**, *13* (1), 60−68.

(13) Yu, J.; Lucas, J.; Wall, T. Modeling the development of char structure during the rapid heating of pulverized coal. *Combust. Flame* **2004**, *136*, 519−532.

(14) Gibbins, J. R.; Kandiyoti, R. The effect of variations in time-temperature history on product distribution from coal pyrolysis. *Fuel* **1989**, *68* (7), 895−903.

(15) Fletcher, T. H.; Hardesty, D. R. *Compilation of Sandia Coal Devolatilization Data: Milestone Report*; Sandia National Laboratories: Livermore, CA, 1992; Report SAND92-8209, p 544.

(16) Chirone, R.; Massimilla, L. The application of Weibull theory to primary fragmentation of a coal during devolatilization. *Powder Technol.* **1989**, *57* (3), 197−212.

(17) Gale, T. K.; Fletcher, T. H.; Bartholomew, C. H. Effects of pyrolysis conditions on internal surface areas and densities of coal chars prepared at high heating rates in reactive and non-reactive atmospheres. *Energy Fuels* **1995**, *9*, 513−524.

(18) Nsakala, N. Y.; Essenhigh, R. H.; Walker, P. L. Characteristics of chars produced from lignites by pyrolysis at 808 °C following rapid heating. *Fuel* **1978**, *57*, 605−611.